

# The passive and active nature of ocean heat uptake in idealized climate change experiments

Peng Xie · Geoffrey K. Vallis

Received: 11 August 2010 / Accepted: 28 March 2011  
© Springer-Verlag 2011

**Abstract** The influence of ocean circulation changes on heat uptake is explored using a simply-configured primitive equation ocean model resembling a very idealized Atlantic Ocean. We focus on the relative importance of the redistribution of the existing heat reservoir (due to changes in the circulation) and the contribution from anomalous surface heat flux, in experiments in which the surface boundary conditions are changed. We perform and analyze numerical experiments over a wide range of parameters, including experiments that simulate global warming and others that explore the robustness of our results to more general changes in surface boundary conditions. We find that over a wide range of values of diapycnal diffusivity and Southern Ocean winds, and with a variety of changes in surface boundary conditions, the spatial patterns of ocean temperature anomaly are nearly always determined as much or more by the existing heat reservoir redistribution than by the nearly passive uptake of temperature due to changes in the surface boundary conditions. Calculating heat uptake by neglecting the existing reservoir redistribution, which is similar to treating temperature as a passive tracer, leads to significant quantitative errors notably at high-latitudes and, secondarily, in parts of the main thermocline. Experiments with larger circulation changes tend to produce a relatively larger magnitude of existing reservoir redistribution, and a faster growing effective heat capacity of the system. The effective heat capacity is found to be sensitive to both vertical diffusivity and Southern Ocean wind.

**Keywords** Ocean heat uptake · Circulation changes · Climate Change · Passive tracer · Effective system heat capacity

## 1 Introduction

Because of its large heat capacity and its role in heat transport, the ocean plays an important role in both slowing down the progression of global warming to its final equilibrium and in influencing the geographical distribution of warming. Consequently, a number of authors have studied ocean heat uptake in order to better address various problems in warming, including the transient climate response (Raper et al. 2001), how the transient climate sensitivity differs from the equilibrium climate sensitivity (Hoffert et al. 1980; Manabe and Stouffer 2007), and the prediction of sea level rise (Church et al. 1991).

A simple and common assumption to make is to suppose, albeit sometimes implicitly, that ocean heat uptake occurs as a passive process. Thus, for example, temperature has been treated to a lesser or greater extent as a passive tracer by Dickinson and Schaudt (1998), Watterson (2000) and Gregory (2000) in various forms of energy balance models, by Wigley and Schlesinger (1985) and Wigley and Raper (1990) in diffusive and upwelling-diffusive models, and by Church et al. (1991) in simple layered models. In this paper we investigate the extent to which a passive tracer treatment is appropriate. An indication that a passive treatment may not be the whole story comes from the work of Banks and Gregory (2006). They compared the uptake of a passive temperature-like tracer to the actual heat uptake in a CO<sub>2</sub> increase experiment using a coupled model, and found that heat uptake was in fact strongly affected by changes in circulation and was rather different from passive tracer uptake.

---

P. Xie · G. K. Vallis (✉)  
AOS Program,  
Princeton University, Princeton, NJ 08544, USA  
e-mail: gkv@princeton.edu

Certainly, the possibility of significant ocean circulation changes in the future warming scenarios cannot be discounted, in particular with regard to changes in the meridional overturning circulation (Manabe and Stouffer 1995, 1999; Dixon et al. 1999; Gregory et al. 2005; Dalan et al. 2005). A weakening of the meridional overturning circulation (MOC) could lead to cooling in the North Atlantic and a warming of the mid-depth tropical and South Atlantic (Vellinga and Wood 2002; Ruhlemann et al. 2004). Observations do indicate some cooling in subpolar regions and slight warming in subtropical regions in the North Atlantic (Arbic and Owens 2001; Lozier et al. 2008), although whether they are related to the MOC weakening is unclear. However, observations (Talley, 1999) suggest that 75% of the total meridional heat transport in the North Atlantic is associated with intermediate and deep water formation, so it is reasonable to assume the MOC weakening would result in important changes in ocean heat transport.

A related issue pertains to the the effective heat capacity,  $C$ , of the ocean and its potential change with global warming. Ocean heat uptake is sometimes discussed using a simple energy balance model of the form  $d(C\Delta T)/dt = F - \lambda\Delta T$ , where  $\Delta T$  is the surface temperature perturbation,  $C$  is the effective, and in general time dependent, system heat capacity,  $F$  is the effective radiative forcing and  $\lambda$  is a climate sensitivity parameter. It may be appropriate to assume that  $C$  is a constant on relatively short time scales (Dickinson and Schaudt 1998; Padilla et al. 2011), although on longer timescales this is not necessarily appropriate (Watterson 2000).

In this paper we investigate the above issues using a simply-configured primitive equation ocean model, changing the boundary conditions and other parameters to investigate how heat is taken up by the ocean. We use such a model because this gives us great experimental control and the ability to cover a broader range of parameters, at the cost of some realism. The model is a very idealized representation of the Atlantic Ocean connected to a re-entrant channel, mimicking the Atlantic Circumpolar Channel, but the Pacific and Indian Oceans are absent, thus to some degree limiting the conclusions we can draw about the real world. The surface boundary conditions are changed both in very idealized ways (e.g., uniform changed in surface relaxation temperature) and using boundary conditions extracted from a global warming experiment with a comprehensive climate model (GFDL's CM2.1). The existing heat reservoir redistribution arising from circulation changes is examined and we compare the actual heat uptake with that obtained by ignoring the existing reservoir redistribution. In its more idealized nature our study is complementary to that of Banks and Gregory

(2006), who performed a much smaller set of experiments but with a more realistic model.

Section 2 is a brief introduction to the model, the utilization of passive tracer, and the experimental design. In Sect. 3, ocean warming is partitioned into contributions from ocean circulation changes and from surface heat flux anomaly, and their influence are compared. Section 4 demonstrates how the system's effective heat capacity is impacted by heat redistribution due to ocean circulation changes. This is followed by a general summary and discussion.

## 2 Numerical model and experimental design

### 2.1 Model introduction

We use a primitive equation ocean model, the Geophysical Fluid Dynamics Laboratory (GFDL) Modular Ocean Model (MOM4p1, Griffies et al. 2004) in a two-hemisphere single-basin, semi-flat bottom, sector configuration. On each boundary is a  $10^\circ$  wide slope going from the surface to the bottom, in order to suppress internal decadal oscillations of the thermohaline circulation, which are often exaggerated in flat-bottom models (Winton 1997). The model extends from  $75^\circ\text{N}$  to  $75^\circ\text{S}$ ,  $55^\circ\text{W}$  to  $5^\circ\text{E}$ , and is about 4,500 m deep. It has a horizontal resolution of  $2.5^\circ \times 2.5^\circ$ , and 24 vertical levels of thickness varying from 25 m at the top to 350 m at the bottom. A convection scheme following Rahmstorf (1993) and a Gent-McWilliams skew flux scheme (Gent and McWilliams 1990) for eddy parameterization are used, and a spatially constant background diffusivity ( $\kappa$ ) is applied everywhere. A simplified Antarctic Circumpolar Channel and Drake Passage are included by way of a zonally-periodic channel extending from  $65^\circ\text{S}$  to  $50^\circ\text{S}$ , partially blocked by topography at depths of 2,500 m and below, as such a feature has a key effect on the ocean structure (Toggweiler and Samuels 1998; Vallis 2000). Thus, the model is configured to be like a very idealized Atlantic Ocean, where the meridional overturning circulation (MOC) is an important component in the heat transport process.

We apply a latitude-dependent wind stress on the ocean surface, as illustrated in Fig. 1. Additionally, the model restores sea surface temperature (SST or  $T_s$ ) and salinity (SSS or  $S_s$ ) to idealized profiles  $T^\star$  and  $S^\star$  respectively, as in Haney (1971), with a thermal restoring coefficient  $\alpha$  of approximately  $40 \text{ W m}^{-2}\text{K}^{-1}$  [the saline restoring coefficient is  $\alpha/C_p$ , where  $C_p = 3,992 \text{ J}/(\text{kg K})$ ]. The surface heat flux  $Q$  and salinity flux  $Q_s$  are thus

$$Q = \alpha(T^\star - T_s), \quad Q_s = \frac{\alpha}{C_p}(S^\star - S_s). \quad (1)$$

For our control runs (denoted CTL, the integrations that give rise to the equilibrium states),  $T^\star$  and  $S^\star$  are annual mean, zonally uniform analytical profiles (Fig. 1) roughly based on the annual global zonal mean observations from the NODC’s World Ocean Atlas 2001 (Conkright et al. 2002). The treatment of surface salinity fluxes is chosen for its simplicity and because it allows us to easily alter the surface boundary conditions, but the hydrology cycle that in reality determines surface salinity is obviously not represented realistically here.

In order to test the sensitivity of the growth rate of effective system heat capacity we conduct two sets of control experiments, varying the vertical diffusivity  $\kappa$  and Southern Ocean wind. In CTL set 1, we use  $\kappa = 1.5 \times 10^{-5} \text{ m}^2/\text{s}$ , and set Southern Ocean (SO) wind stress (33°S to 75°S) equal corresponding Northern Ocean (NO) wind stress multiplied by a factor  $\beta_w$ , where  $\beta_w = 1, 1.5, 2, 2.5$  and 3 (Fig. 1). In CTL set 2, we hold the southern ocean wind stress at twice that of the corresponding northern hemisphere wind ( $\beta_w = 2$ ), while the vertical diffusivity is varied, with values of  $\kappa = 0.5, 1, 1.5, 3$  and  $5 \times 10^{-5} \text{ m}^2/\text{s}$  (see Table 2). All these control experiments are run for about 2,000 years in order to reach equilibrium, with averages typically over the last 100 years used for diagnostics if needed, and then run for an additional 100 years in the perturbation experiments. When differences between the perturbed experiments and the control are diagnosed the same time period is used for both, for example the last 10 years in a 100 year experiment.

The ocean climatology in these experiments is similar to that described in Vallis (2000) and in Fučkar and Vallis (2007), with subtropical and subpolar gyres in the Northern

Hemisphere, and a subtropical gyre and circumpolar flow in the Southern Hemisphere. The overturning circulation includes both an interhemispheric analog of ‘North Atlantic Deep Water’ sourced from high northern latitudes and upwelling in the southern channel, and a still deeper ‘Antarctic Bottom Water’, ventilated in the Southern Ocean. The strength of the circulation of the NADW is determined both by the diapycnal diffusivity and by Southern Ocean winds, increasing with both. The winds over the Southern Ocean particularly affect the inter-hemispheric component, whereas increasing the diapycnal diffusivity tends to enhance the ‘classic’ single-hemisphere, mixing-driven, overturning circulation.

### 2.2 Perturbed experiments

In the perturbed experiments, we change the surface buoyancy fluxes in various ways by adding a temperature and salinity anomaly  $\Delta T^\star$  and  $\Delta S^\star$  to a control run surface temperature and salinity restore profile  $T^\star$  and  $S^\star$  of (1). That is, in the perturbed runs the surface heat flux  $Q$  and salinity flux  $Q_s$  are:

$$Q = \alpha(T^\star + \Delta T^\star - T_s), \quad Q_s = \frac{\alpha}{C_p}(S^\star + \beta_s \Delta S^\star - S_s) \tag{2}$$

Two general types of  $\Delta T^\star$  and  $\Delta S^\star$  forcing are applied for our experiments: (1) time-dependent, latitude-dependent  $\Delta T^\star$  and  $\Delta S^\star$ , calculated using data from global warming experiments in GFDL’s CM2.1, a comprehensive coupled AOGCM described further in Delworth et al. (2006) and Held et al. (2010). These are sets 1–3 in Table 1. (2) Idealized, uniform or latitude-dependent  $\Delta T^\star$ , zero  $\Delta S^\star$  forcing (Fig. 2). These are sets 4 and 5 in Table 1.

For the first type of forcing, we calculate  $\Delta T^\star$  and  $\Delta S^\star$  as follows. First, we obtain monthly data of the Atlantic ocean surface heat flux, SST and SSS anomalies from CM2.1 experiments in which, after the system had equilibrated, CO<sub>2</sub> was instantaneously doubled. (Details of the equilibrium state are given in Delworth et al. 2006 and details of the doubling experiments are given in Held et al. 2010.) These experiments (sets 1–3) have a forcing source denoted CM2.1 2 × CO<sub>2</sub> in Table 1, and the heat flux, temperature and salinity anomalies in CM2.1 are denoted  $\Delta Q_{cm21}$ ,  $\Delta T_{s,cm21}$  and  $\Delta S_{s,cm21}$  respectively. These quantities are used to calculate the corresponding  $\Delta T^\star$  and  $\Delta S^\star$  for use in our experiments, as follows. We suppose that the ocean surface heat flux in CM2.1 experiments,  $Q_{cm21}$ , can, a posteriori, be represented by similar restore condition as in our model and there exists an effective surface restore temperature profile  $T_{cm21}^\star$ . We therefore have  $Q_{cm21} = \alpha(T_{cm21}^\star - T_{s,cm21})$  similar to (1), and  $\Delta Q_{cm21} = \alpha(\Delta T_{cm21}^\star -$

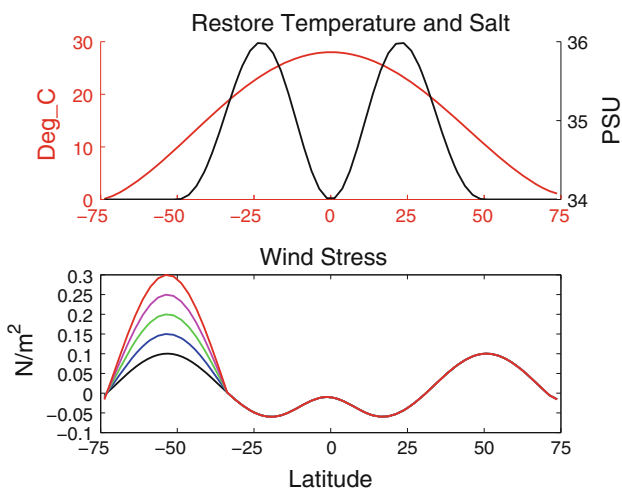


**Fig. 1** Upper surface restore temperature (red) and salinity (black) for control runs. Lower surface wind stress, showing different magnitudes of Southern Ocean wind as used in various different control runs, corresponding to factors of 1,1.5,2,2.5 times the northern hemisphere wind

$\Delta T_{s,cm21}$ ) for the anomaly fields. Using the CM2.1 Atlantic Ocean data, we calculate  $\Delta T_{cm21}^\star$  as

$$\Delta T_{cm21}^\star = \Delta Q_{cm21} / \alpha + \Delta T_{s,cm21} \tag{3}$$

where  $\Delta Q_{cm21}$  and  $\Delta T_{s,cm21}$  are time series and spatial functions for anomalous surface heat flux and SST, and  $\alpha = 40 \text{ W m}^{-2}\text{K}^{-1}$  is the thermal restoring coefficient in our model used in (1). Then we zonally average  $\Delta T_{cm21}^\star$  and

**Table 1** List of perturbed experiments

Experiment name	$\beta_w$	$\kappa$ ( $10^{-5} \text{ m}^2/\text{s}$ )	Forcing source	$\beta_s$
Set 1: varying winds ( $\beta_w$ )				
W1	1	1.5	CM2.1 $2 \times \text{CO}_2$	1
W2	1.5	1.5	CM2.1 $2 \times \text{CO}_2$	1
W3	2	1.5	CM2.1 $2 \times \text{CO}_2$	1
W4	2.5	1.5	CM2.1 $2 \times \text{CO}_2$	1
W5	3	1.5	CM2.1 $2 \times \text{CO}_2$	1
Set 2: varying diffusivity ( $\kappa$ )				
K1	2	0.5	CM2.1 $2 \times \text{CO}_2$	1
K2	2	1.	CM2.1 $2 \times \text{CO}_2$	1
K3	2	1.5	CM2.1 $2 \times \text{CO}_2$	1
K4	2	3	CM2.1 $2 \times \text{CO}_2$	1
K5	2	5	CM2.1 $2 \times \text{CO}_2$	1
Set 3: Varying salinity perturbations				
S1 (same as K3)	2	1.5	CM2.1 $2 \times \text{CO}_2$	1
S2	2	1.5	CM2.1 $2 \times \text{CO}_2$	1/2
S3	2	1.5	CM2.1 $2 \times \text{CO}_2$	1/3
S4	2	1.5	CM2.1 $2 \times \text{CO}_2$	1/4
S5	2	1.5	CM2.1 $2 \times \text{CO}_2$	0
Set 4: uniform $\Delta T^\star$				
set 4_1 to set 4_6	2	1.5	(see Fig. 2)	0
Set 5: latitude-dependent $\Delta T^\star$				
set 5_1 to set 5_8	2	1.5	(see Fig. 2)	0

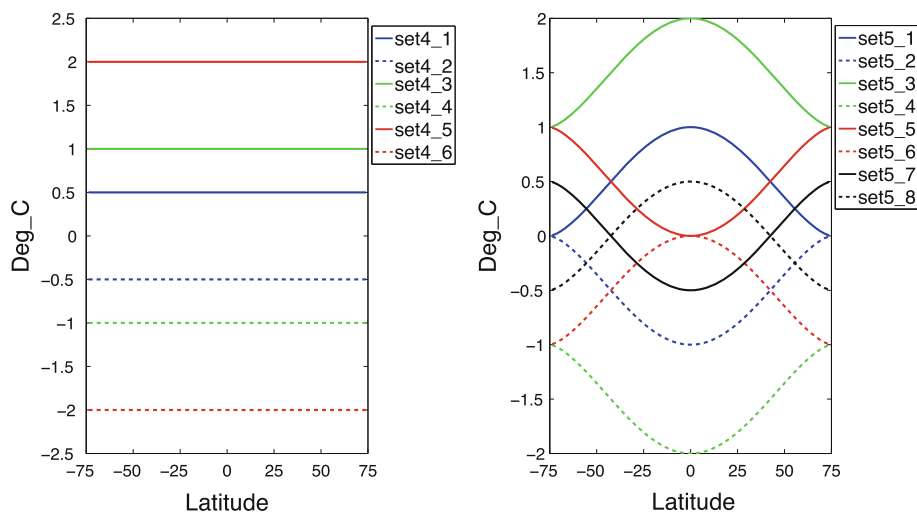
They are based on control runs with different vertical diffusivity  $\kappa$ , or different magnitudes of SO wind stress ( $\beta_w$ ).  $\Delta T^\star$  and  $\Delta S^\star$  forcing are idealized profiles or calculated from the CM2.1  $2 \times \text{CO}_2$  experiment, and for the latter,  $\beta_s$ , the magnitude of  $\Delta S^\star$  forcing [see (2)] are also varied

use it as  $\Delta T^\star$  for our experiments. To calculate  $\Delta S^\star$  we use the sea surface salinity (SSS) anomaly  $\Delta S_{s,cm21}$  in the CM2.1 Atlantic ocean; this is zonally averaged and then directly used as  $\Delta S^\star$  in our model. Note that the calculated  $\Delta T^\star$  and  $\Delta S^\star$  are time-dependent and latitude-dependent as illustrated in Fig. 6.

The various individual experiments differ from each other in Southern Ocean wind stress ( $\beta_w$ ), vertical diffusivity  $\kappa$ ,  $\Delta T^\star$  and  $\Delta S^\star$  forcing, and the magnitude of  $\Delta S^\star$  forcing. Set 1 and set 2 both use  $\Delta T^\star$  and  $\Delta S^\star$  calculated from the CM2.1  $2 \times \text{CO}_2$  integration, but they are applied to CTL runs with varied southern ocean wind (set 1) and vertical diffusivity  $\kappa$  (set 2) in order see how robust the growth of the effective system heat capacity  $C$  is in different regimes. Set 3 is based on a CTL run with the Southern Ocean wind twice as strong as that in the Northern Hemisphere ( $\beta_w = 2$ ) and with  $\kappa = 1.5 \times 10^{-5} \text{ m}^2/\text{s}$ . In this set the salinity forcing is changed. Thus, the  $\Delta T^\star$  forcing is the same for these five integrations, but the magnitude of  $\Delta S^\star$  forcing is multiplied by a factor  $\beta_s$  (where  $\beta_s = 1, 1/2, 1/3, 1/4$  and 0, with the experiments denoted S1 to S5 (see Table 1)). These give different levels of MOC change without directly changing the temperature input.

Set 4 and set 5 both use idealized  $\Delta T^\star$  (Fig. 2) and zero  $\Delta S^\star$  forcing. These perturbations are imposed on the CTL run with the southern ocean wind twice as strong as the corresponding northern hemisphere wind ( $\beta_w = 2$ ) and with  $\kappa = 1.5 \times 10^{-5} \text{ m}^2/\text{s}$ . The  $\Delta T^\star$  is added instantaneously in the beginning of the perturbed runs, and is latitudinally uniform through for set 3 and latitude-dependent for set 4, as in Fig. 2. One feature of these experiments is that for each experiment with a positive temperature forcing perturbation there is an experiment with a negative forcing.

**Fig. 2** Idealized  $\Delta T^\star$  forcing, used in set 4 (left) and set 5 (right) perturbed experiments (see Table 1)



### 2.3 Using a passive tracer to explore heat uptake

We now describe how we use a passive tracer to explore the importance of ocean circulation changes in the heat uptake process using a methodology derived from Banks and Gregory (2006). The ocean temperature field in the non-perturbed state,  $\bar{T}$ , satisfies

$$\frac{\partial \bar{T}}{\partial t} = \bar{F}(x, y, t) - \bar{\mathbf{v}} \cdot \nabla \bar{T}(x, y, z, t) \tag{4}$$

where  $\bar{F}$  is the equilibrium surface heat flux and  $\bar{\mathbf{v}}$  represents all heat transports processes including the parameterized subgridscale velocity. All non-perturbed quantities are marked with overbars and perturbations with primes. (The non-perturbed states are in equilibrium that in principle could be time-dependent, but in practice the time dependence is small.) After a perturbation in the surface conditions there is an anomalous heat flux  $F'$ , which in turn induces a change in temperature,  $T'$ , and a change of circulation,  $\mathbf{v}'$ . The temperature change evolves according to:

$$\frac{\partial T'}{\partial t} = F' - \bar{\mathbf{v}} \cdot \nabla T' - \mathbf{v}' \cdot \nabla \bar{T} - \mathbf{v}' \cdot \nabla T' \tag{5}$$

We now partition the temperature anomaly into two parts: (1)  $T'_r$ , the existing heat reservoir redistribution due to the perturbed circulation; (2)  $T'_a$ , the contribution from anomalous surface heat flux  $F'$ . These are constructed so that the total change in the temperature is equal to the sum of the change due to circulation changes and the change due to surface heat flux anomaly (i.e.,  $T' = T'_r + T'_a$ ). There are of course many ways that the temperature anomaly could be subdivided, but this choice is physically motivated. We thus divide (5) into two parts that satisfy

$$\frac{\partial T'_r}{\partial t} = -\mathbf{v}' \cdot \nabla \bar{T} - \bar{\mathbf{v}} \cdot \nabla T'_r - \mathbf{v}' \cdot \nabla T'_r \tag{6}$$

and

$$\frac{\partial T'_a}{\partial t} = F' - \bar{\mathbf{v}} \cdot \nabla T'_a - \mathbf{v}' \cdot \nabla T'_a \tag{7}$$

Equation (6) shows that  $T'_r$  field evolves because of the presence of the  $-\mathbf{v}' \cdot \nabla \bar{T}$  term. If  $\mathbf{v}' = 0$  then  $T'_r = 0$ . Similarly, (7) shows that the  $T'_a$  field evolves under the driving force of the  $F'$  term: if  $F' = 0$  then  $T'_a = 0$ . The change in  $T'_a$  field is similar but not exactly equal to the heat uptake process with temperature treated as a passive tracer, because of the presence of the small  $\mathbf{v}' \cdot \nabla T'_a$  term.

The above two contributions cannot be evaluated using the thermodynamic equation alone, since this is just one equation for the total temperature, or temperature anomaly  $T' = T'_a + T'_r$ . However, with the help of an appropriate additional passive tracer, we can evaluate the two

components. To this end, we create a passive tracer, that behaves in a similar way to temperature itself, but that allows us to separate  $T_r$  from  $T_a$ . Specifically, the tracer is designed to mimic the behavior of the  $T_r$  field. The tracer, denoted  $P_r$ , has the same initial equilibrium reservoir ( $\bar{P}_r = \bar{T}$ ), the same equilibrium surface flux ( $\bar{F}_{pr} = \bar{F}$ ), and other transport mechanisms as temperature itself. In an unperturbed experiment the tracer satisfies

$$\frac{\partial \bar{P}_r}{\partial t} = \bar{F} - \bar{\mathbf{v}} \cdot \nabla \bar{P}_r, \tag{8}$$

which is the same as (4), so that  $\bar{P}_r = \bar{T}$  at all times. In a perturbed state, where the ocean circulation changes are  $\mathbf{v}'$  and the surface heat flux anomaly is  $F'$ , we keep the surface flux for  $P_r$  unchanged, so the evolution equation of  $P_r = \bar{P}_r + P'_r$  is

$$\frac{\partial P_r}{\partial t} = \frac{\partial (\bar{P}_r + P'_r)}{\partial t} = \bar{F} - \bar{\mathbf{v}} \cdot \nabla (\bar{P}_r + P'_r) - \mathbf{v}' \cdot \nabla (\bar{P}_r + P'_r) \tag{9}$$

Using (8) and (9), the perturbation satisfies

$$\frac{\partial P'_r}{\partial t} = -\mathbf{v}' \cdot \nabla \bar{P}_r - \bar{\mathbf{v}} \cdot \nabla P'_r - \mathbf{v}' \cdot \nabla P'_r \tag{10}$$

Comparing (10) and (6), we see that the anomaly of passive tracer  $P'_r$  equals the existing heat reservoir redistribution  $T'_r$ . That is, a passive tracer  $P'_r$  that satisfies (10) will give us precisely the evolution of  $T'_r$ , which is the redistribution of the existing reservoir  $\bar{P}_r$  when there is only a change in circulation  $\mathbf{v}'$  but no change in surface flux. For this reason  $T'_r$  is called the “existing heat reservoir redistribution”.

The actual algorithm we use is as follows. We step forward the passive tracer equation (9) to give  $P_r$ , using the surface flux  $\bar{F}$  from the CTL runs, but advecting with the full (perturbed) velocity field  $\mathbf{v} = \bar{\mathbf{v}} + \mathbf{v}'$ . The existing heat reservoir redistribution  $T'_r$  is then given by  $T'_r = P'_r = P_r - \bar{P}_r = P_r - \bar{T}$ , using the perturbed experiments. The evolution of  $T'_a$  [(7)] is obtained from  $T'_a = T' - T'_r$ . [As a check, in some cases we also integrated a passive tracer obeying (7), to ensure that  $T'_a + T'_r = T'$ . However, one need only introduce one additional passive tracer to separate  $T'_a$  from  $T'_r$ .] At the initial time  $T'_r = T'_a = 0$ . In the next few sections we discuss the relative importance of  $T'_a$  and  $T'_r$  in a range of numerical experiments.

### 3 Geographical redistribution of heat due to ocean circulation changes

In this section we focus on one of our perturbation experiments from Set 3, namely S1 (see Table 1). This is based on a control run with the Southern Ocean wind twice

as strong as that in the Northern Hemisphere ( $\beta_w = 2$ , the green line in the lower panel of Fig. 1), and with background diffusivity  $\kappa = 1.5 \times 10^{-5} \text{ m}^2/\text{s}$ . For  $\Delta S^*$  forcing,  $\beta_s = 1$  is used. The buoyancy forcing is derived from an experiment of the comprehensive climate model CM2.1 in which  $\text{CO}_2$  was doubled instantaneously and the perturbation temperature and salinity forcing fields  $\Delta T^*$  and  $\Delta S^*$  for the idealized experiments then calculated as described above. Using the passive tracer technique we then calculate the temperature change  $T'$ ,  $T'_r$  the existing heat reservoir redistribution, and  $T'_a$  the contribution from anomalous surface heat flux  $F'$  separately. Figure 3 shows the zonal mean  $T'$ ,  $T'_r$  and  $T'_a$  fields, averaged for the last 10 years of the 100 year simulation.

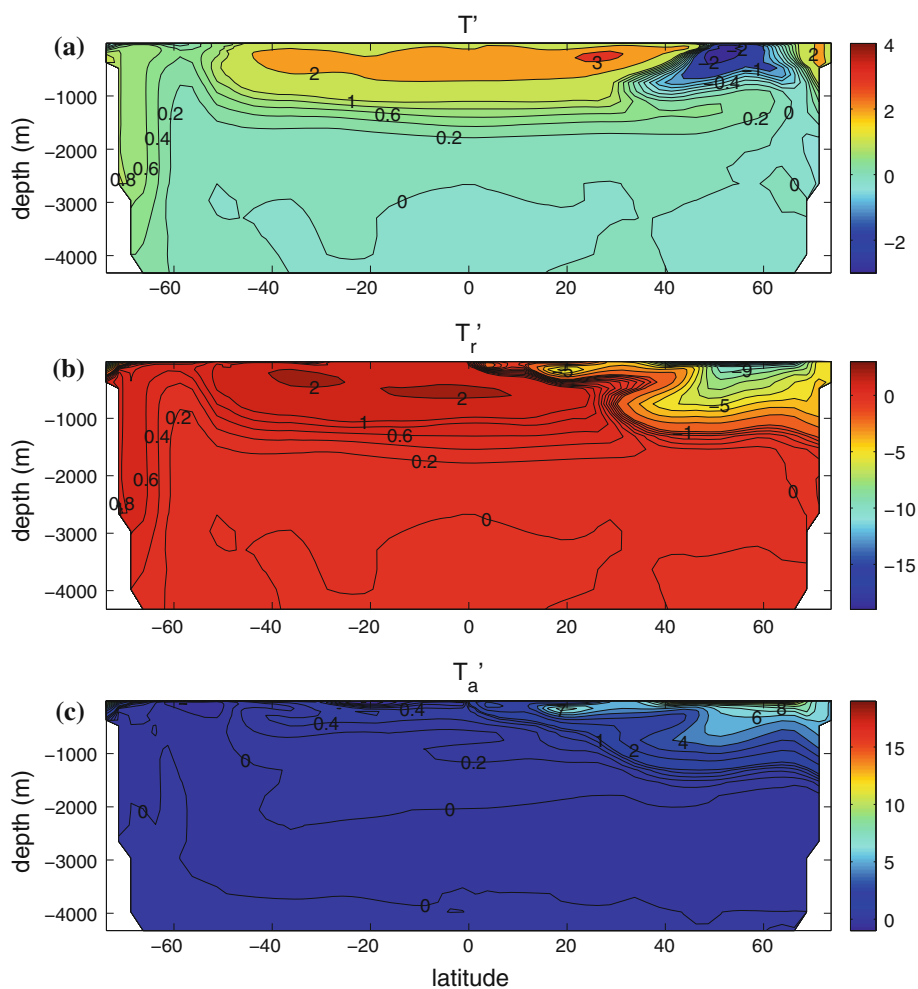
### 3.1 Patterns of ocean warming

Focusing on the total temperature change  $T'$  (upper panel in Fig. 3), there are 3 evident features: cooling in the Northern Hemisphere high latitudes, warming in the main thermocline and slight warming through the whole column in the Southern Hemisphere high latitudes except for a slight cooling in the surface. The contribution from the anomalous surface heat flux ( $T'_a$ , lower panel in Fig. 3) also contributes to the warming of main thermocline. It also causes slight warming in Southern Hemisphere high-latitude surface and rather intense warming in the Northern Hemisphere high latitudes. Overall,  $T'_r$ , the redistribution of the existing heat reservoir by the circulation changes, is the

except at the surface in Southern Hemisphere high latitudes. Those features are also the most obvious ones in the warming of the Atlantic Ocean in the actual CM2.1  $2 \times \text{CO}_2$  experiment (Fig. 4). Evidently, if the forcing is constructed appropriately, our ocean model undergoes somewhat similar changes as the more complicated CM2.1 model which gives us confidence that our calculations have relevance to the results of comprehensive coupled models, and possibly the real climate system (5).

The existing heat reservoir redistribution ( $T'_r$ , the middle panel in Fig. 3) shows a large cooling in the Northern Hemisphere high latitudes, a warming in the main thermocline, a slight warming through the whole column in the Southern Hemisphere high latitudes except for a slight cooling in the surface. The contribution from the anomalous surface heat flux ( $T'_a$ , lower panel in Fig. 3) also contributes to the warming of main thermocline. It also causes slight warming in Southern Hemisphere high-latitude surface and rather intense warming in the Northern Hemisphere high latitudes. Overall,  $T'_r$ , the redistribution of the existing heat reservoir by the circulation changes, is the

**Fig. 3** Perturbation temperatures in the S1 experiment ( $\kappa = 1.5 \times 10^{-5} \text{ m}^2/\text{s}$ ,  $\beta_w = 2$  and  $\beta_s = 1$ , see Table 1). **a** Actual zonal mean ocean temperature change  $T'$  in 10th decade. **b** Zonal mean existing heat reservoir redistribution  $T'_r$  in 10th decade. **c** Zonal mean contribution from anomalous surface heat flux  $T'_a$ , in 10th decade. The interval of contours is generally  $1^\circ\text{C}$  with  $0.2^\circ\text{C}$  interval between the  $[-1^\circ\text{C}, 1^\circ\text{C}]$  range



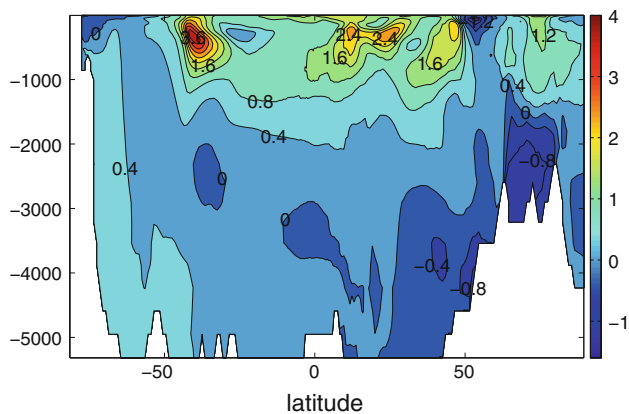


**Fig. 4** GFDL’s CM2.1 CO<sub>2</sub> doubling experiment (CM2.1 2 × CO<sub>2</sub> integration), Atlantic Ocean, zonal mean temperature anomaly  $T'$  in 10th decade. The interval of contours is 0.4°C.

dominant contributor of the three main features of ocean warming in our model. This shows especially in the Northern Hemisphere high-latitude upper ocean. The generally opposing effects of anomalous heat input and existing redistribution are broadly consistent with the prior results of Lowe and Gregory (2006). As something of an aside, we note that although the surface restore temperature leads to a slight cooling at high northern latitudes (Fig. 6), the actual cooling is mainly due to the existing reservoir redistribution  $T'_r$  while surface heat flux anomaly is warming the area, mainly because of advective effects. It, though, worth noticing that  $T'_r$  is cooling the ocean surface significantly (the red line in the middle panel of Fig. 7), so  $T'$  on the surface is cooler than it could be if there was no existing reservoir redistribution (then  $T' = T'_a$ ).

### 3.2 Details of the redistribution of the existing heat reservoir

For Southern Hemisphere high latitudes the temperature distribution is greatly affected by deep convection in the equilibrium state. In the perturbed experiments the deep convection is weakened, causing a slight cooling in Southern Hemisphere high latitudes surface and a warming at depth, in the  $T'_r$  field. The warming extends almost to the bottom of the ocean in the region of the circumpolar channel. In the northern hemisphere ocean subsurface temperature changes arise from the weakening of MOC (red line in left panel, Fig. 7). The MOC strength is represented by the maximum of overturning stream function, and we define the ‘MOC change ratio as the percentage of MOC strength change averaged over the last 50 years in every perturbed runs (positive values mean MOC weakening). The MOC weakening leads to a reduction of the northward heat transport in the upper Northern Hemisphere ocean, and a fairly intense cooling in high latitudes near the

surface. The surface cooling is also propagated into deeper layers by convection in the Northern Hemisphere high latitudes, which shows a cooling extending over 1,000 m in the  $T'_r$  field (Fig. 3). For low latitudes the decrease of MOC strength leads to reduced upwelling of cold water, which is why the main thermocline warms in the  $T'_r$  field.

It is interesting to see how the ocean circulation changes redistributes heat meridionally and vertically. Figure 5 shows the volume-averaged  $T'_r$  for three meridionally divided regions and three vertically divided regions. We see that  $T'_r$  falls steadily northward of 40°N and rises slightly between 40°N and 40°S, and southward of 40°S. In addition,  $T'_r$  is falling in the upper ocean (above 400 m), substantially increasing in intermediate waters (400–1,400 m) and slightly increasing in the abyss. Put simply, ocean circulation changes are redistributing the existing heat reservoir from the surface to the intermediate and deep ocean vertically, and from the Northern Hemisphere high latitudes to the tropics and the Southern Hemisphere meridionally.

Note that although our experiment S1 has a larger Atlantic MOC change ratio ( $\approx 50\%$ ) than the actual CM2.1 2 × CO<sub>2</sub> experiment ( $\approx 30\%$ ), similar experiments that have more modest MOC change (e.g., magenta line in left panel, Fig. 7) do inherit nearly all features of  $T'_r$  we described above, albeit with a smaller magnitude.

### 3.3 Comparison of $T'_r$ and $T'_a$ across different experiments

The experiments we have performed give us a wide range of ocean circulation transient changes, and we would like to compare the contributions from the  $T'_r$  and  $T'_a$  fields in a compact way.

To this end, we will denote the the spatial root mean square magnitude of  $T'_r$ ,  $T'_a$  and  $T'$  by  $S_r$ ,  $S_a$  and  $S$ , and we denote the spatial correlation between  $T'_r$  and  $T'$ ,  $T'_a$  and  $T'$  by  $R_r$  and  $R_a$ , respectively. Thus, we define:

$$S_r \equiv \left[ \frac{1}{V} \int T'_r(x_i, t)^2 dx_i \right]^{1/2},$$

$$S_a \equiv \left[ \frac{1}{V} \int T'_a(x_i, t)^2 dx_i \right]^{1/2}, \tag{11}$$

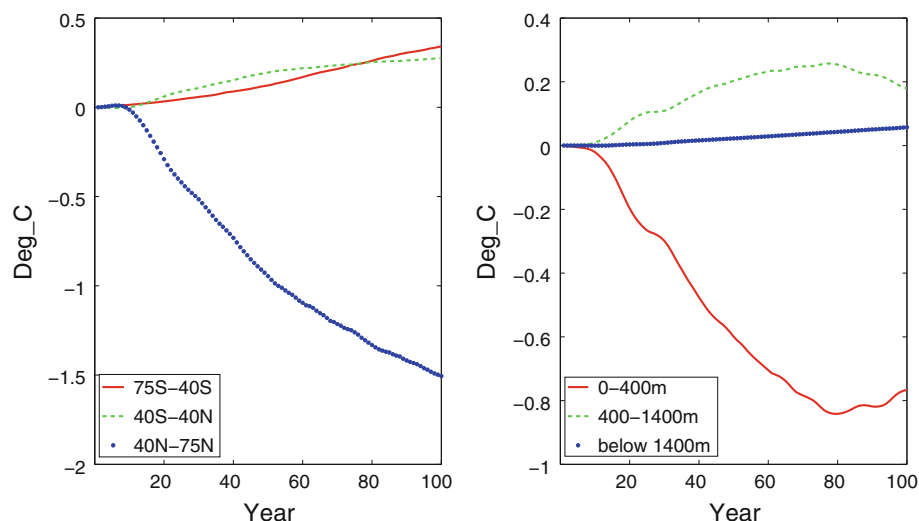
$$S \equiv \left[ \frac{1}{V} \int T'(x_i, t)^2 dx_i \right]^{1/2}, \tag{12}$$

and

$$R_r = \frac{\int T'_r(x_i, t) \times T'(x_i, t) dx_i / V}{S_r \times S},$$

$$R_a = \frac{\int T'_a(x_i, t) \times T'(x_i, t) dx_i / V}{S_a \times S} \tag{13}$$

**Fig. 5** Volume mean  $T'_r$  time series in S1 integration ( $\kappa = 1.5 \times 10^{-5} \text{ m}^2/\text{s}$ ,  $\beta_w = 2$  and  $\beta_s = 1$ , see Table 1). *Left* the ocean is meridionally divided into 3 areas, using  $40^\circ\text{S}$  and  $40^\circ\text{N}$  as boundaries. *Right* the ocean is vertically divided into 3 areas, using 400 and 1,400 m as boundaries



where  $\int dx_i$  means integration over all three spatial dimensions and  $V$  is the total ocean volume. We do not subtract the mean of the values before taking the correlation in order that this reflect the overall sign of the effect, and so the above resembles the ‘anomaly correlation coefficient’ used in weather forecasting.

In Fig. 8 we show  $R_r$ ,  $R_a$ ,  $S_r$  and  $S_a$ , averaged in the last 50 years, for every perturbed experiments listed in Table 1, as a function of the MOC change ratio (the percentage change in MOC strength, with positive values denoting a weakening). Generally both  $S_r$  and  $S_a$  have a very roughly linear relationship with the MOC change ratio (middle panel of Fig. 8). In particular, the existing reservoir redistribution is dominated by the MOC change and the larger MOC change, the larger  $T'_r$  change. Second, in nearly all the perturbed experiments, the ratio between  $S_r$  and  $S_a$  is about equal to or greater than one, the exceptions being two experiments where the MOC change is very small and the MOC change ratio is close to zero (lower panel in Fig. 8). Except in those two experiments,  $R_r$ , the spatial correlation between  $T'_r$  and  $T'$ , is obviously larger than  $R_a$ , the spatial correlation between  $T'_a$  and  $T'$  (upper panel in Fig. 8). That is to say,  $T'_r$  has a greater effect than  $T'_a$  in defining the spatial structure of  $T'$ , except when the circulation changes are very weak. Even in those two experiments of small circulation changes,  $R_r$  is above 0.3 and  $S_r/S_a$  is about 0.5 so that the contribution from  $T'_r$  to  $T'$  is still substantial.

In summary, in our model simulations the existing heat reservoir redistribution due to circulation changes is mainly influenced by the MOC change. It is this that mainly determines the high-latitude temperature changes and enhances the warming of low latitude intermediate water. In the vertical, the existing reservoir redistribution cools the surface and warms the intermediate water. Meridionally, the redistribution serves to transport heat from the Northern Hemisphere high latitudes to the tropics and the

Southern Hemisphere (Fig. 5). Across experiments with a wide range of ocean circulation changes, except when the circulation changes are really small,  $T'_r$ , the existing heat reservoir redistribution, usually plays a more significant role than  $T'_a$ , the contribution from anomalous surface heat flux, in determining the overall temperature change  $T'$ . A consistent result was found by Banks and Gregory (2006) in a more comprehensive model, and a discussion of why this might be so is given in the Sect. 5.

#### 4 The influence of ocean circulation changes on the effective heat capacity of the system

In the widely-used simple energy balance model  $d(CT)/dt = F - \lambda T$ , the ocean’s role is crudely represented by  $d(C \times T)/dt$  term, where  $C$  is the effective, and in general time-dependent, heat capacity of the system. Different assumptions have been made and various results found about the heat capacity, albeit sometimes with different purposes in mind. Thus, sometimes  $C$  is assumed constant (Dickinson and Schaudt 1998), although  $C$  was been found to be approximately linearly increasing with time under monotonically increasing forcing  $F$  (Watterson 2000). Sometimes the rate of heat content change is taken as proportional to surface temperature anomaly  $T'$ , so that that  $d(CT)/dt \approx \kappa_c T'$  where  $\kappa_c$  is a constant (Gregory and Mitchell 1997), and sometimes it is taken as proportional to surface and deep ocean temperature anomaly difference so that  $d(C \times T)/dt \approx \gamma(T' - T'_d)$ , where  $\gamma$  is a constant and  $T'_d$  is deep ocean temperature anomaly (Gregory 2000).

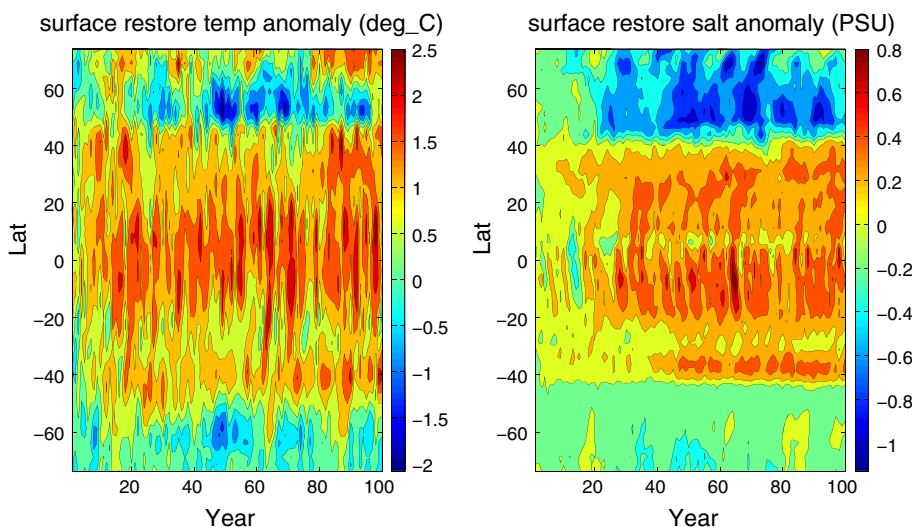
We might intuitively expect the effective heat capacity of the ocean to increase as longer timescales come into play, because heat anomalies can then propagate further into the ocean. In a simple diffusive model undergoing

oscillatory forcing, for example, the depth of influence of a change in the surface boundary conditions increases with the square root of the period of the forcing, and Keen and Murphy (1997) found that the vertical transfer of heat in an ocean model corresponded reasonably well with a diffusive model. A two-box model (e.g., Raper et al. 2002) was found by Held et al. (2010) to be very useful in interpreting climate change experiments with a comprehensive GCM, as well as providing a useful way to estimate transient climate sensitivity from observations (Padilla et al. 2011). In such a model the upper box, representing the mixed layer, responds very quickly to a change in forcing—on the time scale of a few years to a decade—whereas the deep ocean takes hundreds to thousands of years to equilibrate. Perhaps surprisingly, on the decadal timescale both the historical record and the future warming of a GCM can be simulated very well by a single box representing the mixed layer, but on longer timescales the deep ocean begins to warm and so the effective heat capacity increases, and on centennial and longer timescales the heat capacity certainly cannot be regarded as a constant. In reality the ocean is neither diffusive nor a two-box model, although it may be possible to model the effective heat capacity relatively simply (Watterson 2000).

Our goal here is to investigate if and how the effective heat capacity of our system does vary in time in our climate change experiments. We compute the effective depth of the ocean  $H_e$  following the convention of Watterson (2000). That is,  $H_e$  equals the spatially integrated temperature anomaly of our ocean, divided by the anomaly of mean SST,  $T'_s(t)$ , and ocean surface area  $A$  (we assume a constant density  $\rho_0 = 1,035 \text{ kg/m}^3$  everywhere, since the variation of sea water density is very small):

$$H_e(t) = \frac{1}{A} \int T'(x_i, t) dx_i / T'_s(t) \tag{14}$$

**Fig. 6** Time-latitude panels for 100 years of  $\Delta T^*$  and  $\Delta S^*$  forcing, calculated from CM2.1  $2 \times \text{CO}_2$  integration. *Left* surface restore temperature anomaly  $\Delta T^*$ . *Right* surface restore salinity anomaly  $\Delta S^*$  ( $\beta_s = 1$ ). Both fields are zonally uniform



From this definition we see that  $H_e(t) = C(t)/(A\rho_0 C_p)$ , where  $C_p = 3,992 \text{ J/(kg K)}$ . Note that  $H_e$  may be time-dependent.

#### 4.1 Heat capacity with different transient ocean circulation responses

We first look at how  $H_e$  changes under different magnitudes of transient ocean circulation changes. Based on the control integratin with  $\kappa = 1.5 \times 10^{-5} \text{ m}^2/\text{s}$  and  $\beta_w = 2$  (the green line in the lower panel of Fig. 1), we apply the perturbation forcing calculated using the CM2.1  $2 \times \text{CO}_2$  simulation (Fig. 6), in which the  $\text{CO}_2$  level was instantaneously doubled and then kept constant. We also perform integrations in which we vary the magnitude of  $\Delta S^*$  forcing by a factor  $\beta_s$  and produce perturbed runs S1 to S5 (Table 1). Because we use the same temperature ( $\Delta T^*$ ) forcing, all the five experiments end up with about the same SST changes. However, the different salinity ( $\Delta S^*$ ) forcing induces different ocean circulation changes, which in our ocean model are most obvious in the magnitude of MOC changes (left panel of Fig. 7). We find that  $H_e$  generally grows with time (right panel in Fig. 7), and that the growth rate of  $H_e$  has a positive correlation with the magnitude of MOC change: the larger MOC change, the faster  $H_e$  grows.

In Sect. 3 we noted that using the forcing calculated from the CM2.1  $2 \times \text{CO}_2$  simulation the existing heat reservoir redistribution cools the ocean surface and warms the intermediate water, and meridionally it cools the high-latitude surface (especially the Northern Hemisphere) and warms the mid-latitudes and tropics. In addition we have shown that the magnitude of  $T'_r$  changes is dependent on the magnitude of MOC changes. This suggests two processes may be occurring. First, we see that with larger

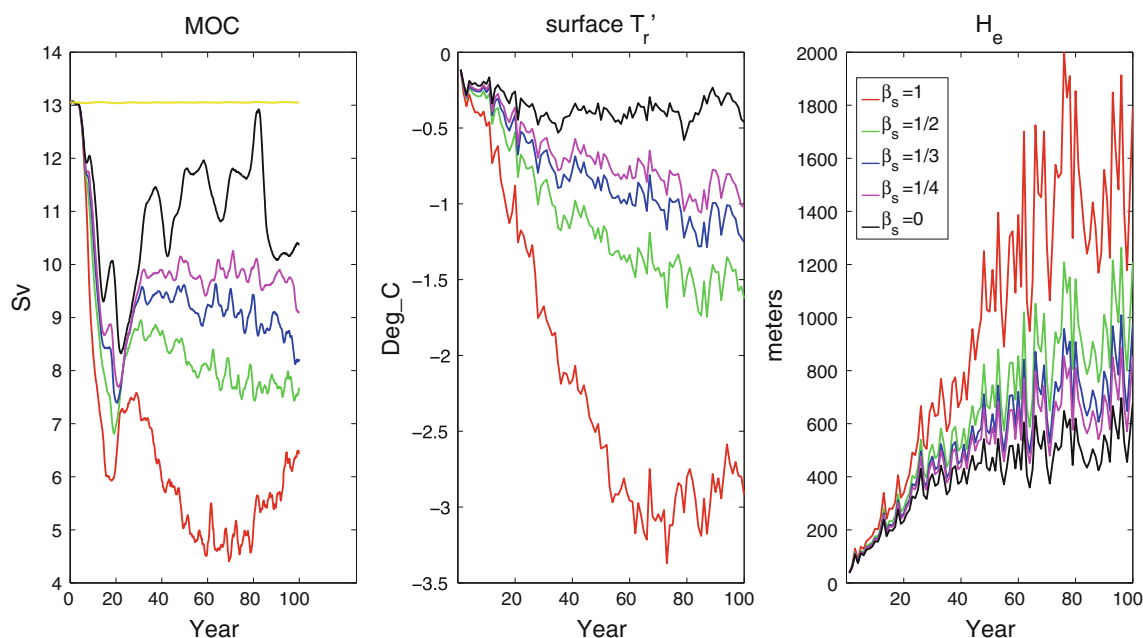


**Fig. 7** Integrations with  $\Delta T^*$  and  $\Delta S^*$  forcing calculated from the CM2.1  $2 \times \text{CO}_2$  experiment, and varied  $\beta_s$  (S1 to S5 in Table 1). *Left* MOC strength (maximum of overturning stream function), *yellow line*

MOC change  $T'_r$  the existing reservoir redistribution is cooling the surface more intensively (middle panel in Fig. 7), and thus more heat can be absorbed into the ocean, resulting in a faster growth of the ocean effective depth  $H_e$ . Second, the larger MOC change will lead to a greater high-latitude surface existing reservoir cooling, and thus more anomalous surface heat input would be concentrated in high latitudes, where heat is generally propagated deeper than in mid and low latitudes. This mechanism also leads to faster growing  $H_e$ , as is evident in Fig. 9, the comparison between MOM  $2 \times \text{CO}_2_{\text{s1}}$  integration and  $2 \times \text{CO}_2_{\text{s4}}$  integration. The dotted lines in the lower panel in Fig. 9 show what  $H_e$  would be if we keep the surface anomalous heat flux distribution, but stop the ocean circulation from changing ( $v' = 0$ , and thus  $T'_r = 0$ ), which means the ocean is taking up the heat flux exactly like a passive tracer. Note that between these two experiments, the MOM  $2 \times \text{CO}_2_{\text{s1}}$  integration has a larger MOC weakening, and thus its surface anomalous heat input is higher in high latitudes compared to MOM  $2 \times \text{CO}_2_{\text{s4}}$  integration. Without circulation changes,  $T'_r$  would be zero everywhere, but  $H_e$  still grows faster in the S1 integration than in the S4 integration due to more concentrated anomalous surface heat input in high latitudes.

A related point is that if we keep the same surface anomalous heat flux and ocean circulation changes, but do not consider the existing heat reservoir redistribution (that is, use  $T'_a$  to represent  $T'$ ), we obtain a more slowly growing  $H_e$ , as shown in the lower panel of Fig. 9 and in

is the CTL run MOC strength. *Middle* the existing heat reservoir redistribution  $T'_r$  averaged through the surface layer. *Right* ocean effective depth  $H_e$

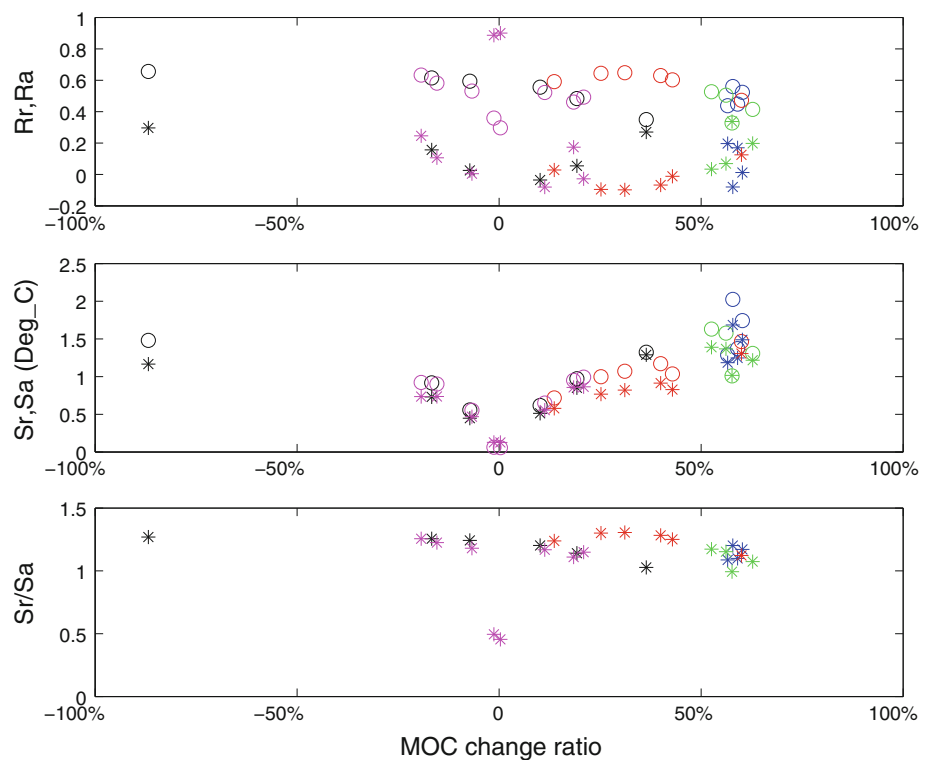
Fig. 10: the dashed lines ( $H_e$  calculated using only the  $T'_a$  field) are much smaller than the solid lines at the end of the experiments. Ocean circulation changes tend to increase the system effective depth  $H_e$  by enhancing the transport of the existing heat reservoir from the upper to the deeper ocean (see in  $T'_r$  field). Neglecting the effects of changes in the existing heat reservoir redistribution leads to quantitative errors in the effective heat capacity of the climate system, at least in our model.

Thus, to summarize, we find that the effective depth  $H_e$  and thus the effective heat capacity of the system, grows with time after the forcing has increased. Ocean circulation changes evidently influence the effective system heat capacity growth rate in two ways: (a) they allow more heat to be absorbed into the ocean by reducing the overall SST, (b) they increase the heat penetration depth by reducing high-latitude surface heat loss, through cooling the high-latitude surface. Generally, larger ocean circulation changes increase the growth rate of effective system heat capacity  $C$ , and potentially slow down the warming process of the atmosphere-ocean coupled system. And, perhaps most germanely, significant errors arise if we only consider the contribution from anomalous surface heat flux ( $T'_a$ ) and leave out the existing heat reservoir changes ( $T'_r$ ).

#### 4.2 Heat capacity with different background conditions

The growth of ocean effective depth  $H_e$  is not only sensitive to the forcing, but also sensitive to background vertical

**Fig. 8** Upper the spatial correlation between  $T'_r$  and  $T'$  ( $R_r$ , circles),  $T'_a$  and  $T'$  ( $R_a$ , stars) as defined in (11), averaged in the last 50 years for all the perturbed experiments listed in Table 1. Green for set 1, blue for set 2, red for set 3, black for set 4, magenta for set 5. Middle the spatial mean magnitude of  $T'_r$  ( $S_r$ , circles) and  $T'_a$  ( $S_a$ , stars) as defined in (3), averaged in the last 50 years of experiments. Lower ratio between last 50 years' mean  $S_r$  and  $S_a$



diffusivity and Southern Hemisphere wind. We again consider experiments using perturbation forcing calculated from the CM2.1  $2 \times \text{CO}_2$  integration, but they are based on different control runs in which the Southern Ocean wind (set 1) and constant vertical diffusivity (set 2) are varied (Table 1).

Overall, we find that higher diffusivity and larger SO wind stress both lead to stronger MOC in the control runs, which is consistent with standard theory (described, for example, in Vallis 2006, chapter 15). After perturbing the surface conditions, we additionally find that the absolute value of MOC change has a positive correlation with diffusivity and the Southern Ocean wind stress. However, the MOC change ratio remains almost constant with different diffusivity or SO wind (Table 2). This is consistent with theory as the MOC change ratio should be largely decided by the change of meridional buoyancy gradient or change in winds. Since we used the same control run and perturbed forcing profiles of  $T^\star$  and  $S^\star$ , we would expect same ratio of MOC change in all these integrations.

From Fig. 10, we can see that an ocean with higher vertical diffusivity or larger Southern Ocean wind stress tends to have faster growing effective depth under the same forcing. Also, larger MOC change due to higher diffusivity or stronger SO wind tends to lead to more intense high-latitude surface cooling in  $T'_r$  field, which will induce more surface anomaly heat input there (Fig. 11). As we explained in Sect. 4.1, more concentrated surface anomalous heat input in high latitudes would result in faster

growing  $H_e$ . Generally, we find that with higher diffusivity or larger Southern Ocean wind stress, our ocean model tends to produce larger MOC weakening during warming, consistent with theory that suggest that the fractional change in the MOC is proportional the diffusivity and/or Southern winds. A weaker MOC tends to cool down the high-latitude surface and so allow the absorption of more heat into the deep ocean, leading in turn to a faster growing effective system heat capacity.

#### 4.3 Nonlinearity of the response of the model under idealized forcing

In our more idealized forcing experiments (set 4 and set 5) each experiment is paired with another with the opposite value of  $\Delta T^\star$  forcing (Fig. 2), in order to study possible nonlinear differences between heating and cooling. Thus, set 4 comprises three warming experiments and three cooling experiments, and set 5 includes four experiments with an increasing equator-to-pole surface buoyancy gradient and four with a decreasing gradient.

We first note that the magnitude of the transient MOC strength change in the perturbed states is largely dependent on the value of high-latitude forcing and is less sensitive to the overall change of equator-to-pole surface buoyancy gradient (essentially because the MOC does not ‘see’ the surface conditions in lower latitudes because of the buffering effect of the main thermocline, as discussed by Samelson and Vallis 1997). Examination of Fig. 2 and Fig.

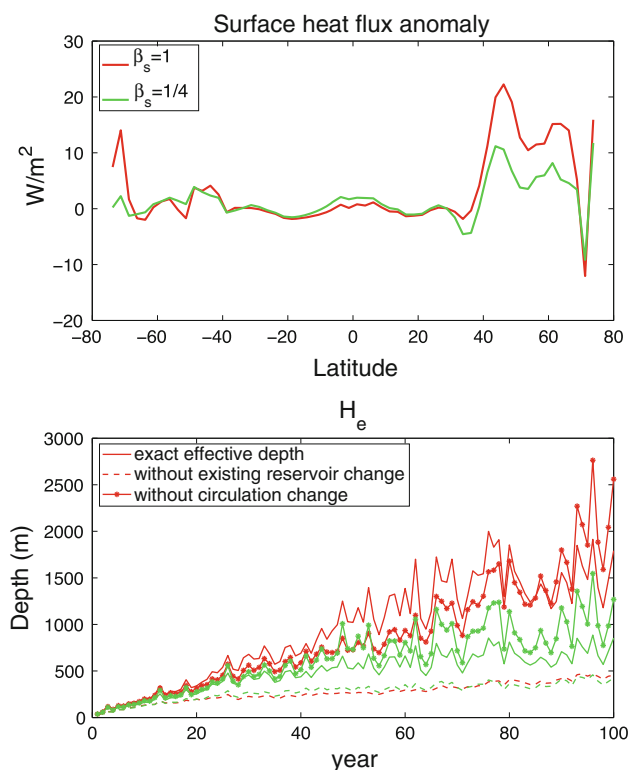


**Fig. 9** Integrations with the  $\Delta T^*$  and  $\Delta S^*$  forcing calculated from the CM2.1  $2 \times \text{CO}_2$  experiment with  $\beta_s = 1$  (red) and  $\beta_s = 1/4$  (green) (S1 and S4 in Table 1). Upper 100 years mean, zonal mean surface heat flux anomaly. Lower ocean effective depth  $H_e$ , solid lines are for actual effective depth, dashed lines are for  $H_e$  calculated without existing reservoir change (assuming  $T'_r \equiv 0$ ) and dotted lines are for  $H_e$  in integrations without ocean circulation changes ( $v' = 0$ , and thus  $T'_r = 0$  and  $T'_a$  is passively advected)

12 indicates that positive high-latitude  $\Delta T^*$  forcing induces a weakening of MOC and negative high-latitude  $\Delta T^*$  forcing leads to MOC strengthening. Experiments with a larger magnitude of high-latitude  $\Delta T^*$  forcing result in a greater MOC change, while experiments with similar high-latitude  $\Delta T^*$  forcing lead to a similar MOC response even when the difference between their equator  $\Delta T^*$  forcing values is as high as  $2^\circ\text{C}$  (e.g., experiments 5\_3 and 5\_5 in the middle panel of Fig. 12).

We also find that our ocean responses are generally non-linear, in that there are greater transient responses to cooling than to warming in set 4 experiments (left panel of Fig. 12). Experiments of set 5 with negative and positive high-latitude  $\Delta T^*$  forcing show a similar effect, and using a comprehensive coupled model Stouffer (2004) also found that the equilibrium response was achieved more rapidly in experiments in which carbon dioxide was halved than when it was doubled, with exceptions in the Atlantic ocean because of changes in the meridional overturning circulation. This nonlinearity shows in the growth rate of effective system heat capacity. In the right panel of Fig. 12, cooling experiments tend to have faster growing ocean effective depth  $H_e$  and thus faster growing effective system heat capacity than corresponding warming experiments. A closer analysis reveals that the influence on  $H_e$  from neither the existing reservoir redistribution  $T'_r$  nor the contribution from anomalous surface heat flux  $T'_a$  are equal and opposite between warming and cooling experiments because the ocean circulation changes are different.

Considering the  $T'_r$  field first, as we mentioned in Sect. 4.1, the redistribution of the existing heat reservoir increases the growth rate of  $H_e$  in the warming experiments by cooling the ocean surface and concentrating anomalous surface heat input in high latitudes. Meanwhile in the cooling scenarios,  $T'_r$  is warming the high latitudes and cooling the main thermocline, which are opposite to the warming scenarios (middle panels in Figs. 13 and 14). The high-latitude  $T'_r$  warming also helps concentrate anomalous surface heat loss in high latitudes and increases the overall penetration depth of cooling anomaly. But unlike in the warming scenarios where the high-latitude  $T'_r$  cooling dominates the surface mean  $T'_r$ , now the low-latitude  $T'_r$  cooling dominates, as the high-latitude  $T'_r$  warming is advected into deeper ocean due to strengthened and deepened MOC. This fact helps decrease the mean SST in the cooling scenarios (not shown), which could reduce the mean heat loss from the surface and decrease the effective system heat capacity growth rate. In summary, the existing heat reservoir redistribution  $T'_r$  results in faster growth of effective system heat capacity in the warming experiments. But in the cooling scenarios,  $T'_r$  helps accelerate and slow

**Table 2** Control runs and perturbed runs MOC strength in set 1 and set 2 experiments

Set 1: $\beta_w$	$\Delta\text{MOC}(\text{Sv})/\text{MOC}_{\text{ctl}}(\text{Sv})$	Set 2: $\kappa (\times 10^{-5} \text{ m}^2/\text{s})$	$\Delta\text{MOC}(\text{Sv})/\text{MOC}_{\text{ctl}}(\text{Sv})$
1	3.98/8.30 $\approx 48\%$	0.5	5.45/11.40 $\approx 48\%$
1.5	5.78/11.13 $\approx 52\%$	1	6.13/12.27 $\approx 50\%$
2	6.62/13.05 $\approx 51\%$	1.5	6.62/13.05 $\approx 51\%$
2.5	7.21/15.04 $\approx 48\%$	3	7.84/15.39 $\approx 51\%$
3	7.68/16.99 $\approx 46\%$	5	9.07/18.28 $\approx 50\%$

MOC strength is indicated by the maximum of overturning stream function.  $\Delta\text{MOC}$  is defined by  $\text{MOC}_{\text{ctl}}$  minus averaged MOC strength in the last 50 years of perturbed runs

**Fig. 10** Integrations with the  $\Delta T^*$  and  $\Delta S^*$  forcing calculated from the CM2.1  $2 \times \text{CO}_2$  experiment, but based on control runs with different southern ocean wind (*left*) and vertical diffusivity (*right*, sets 1 and set 2 in Table 1 respectively). *Solid lines* true effective depth  $H_e$ ; *dashed lines*  $H_e$  without existing reservoir change (take  $T'_r \equiv 0$ )

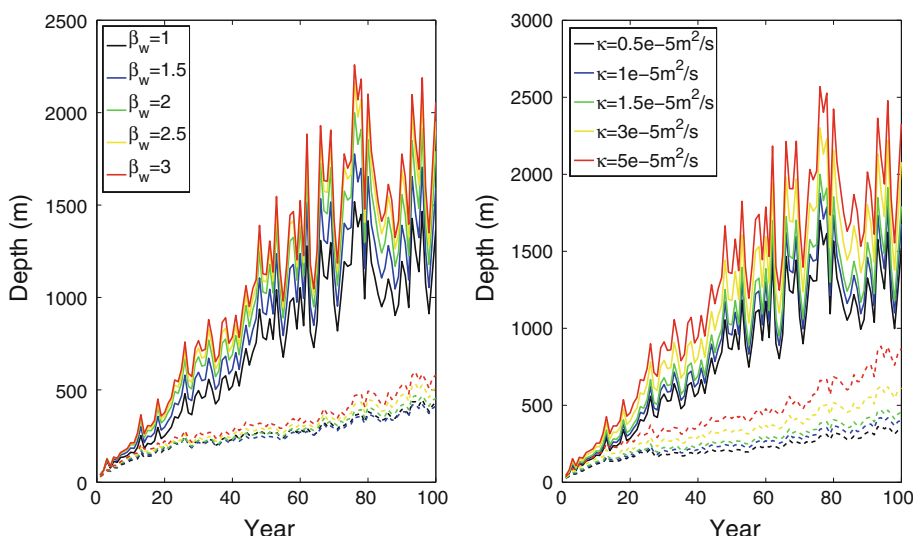
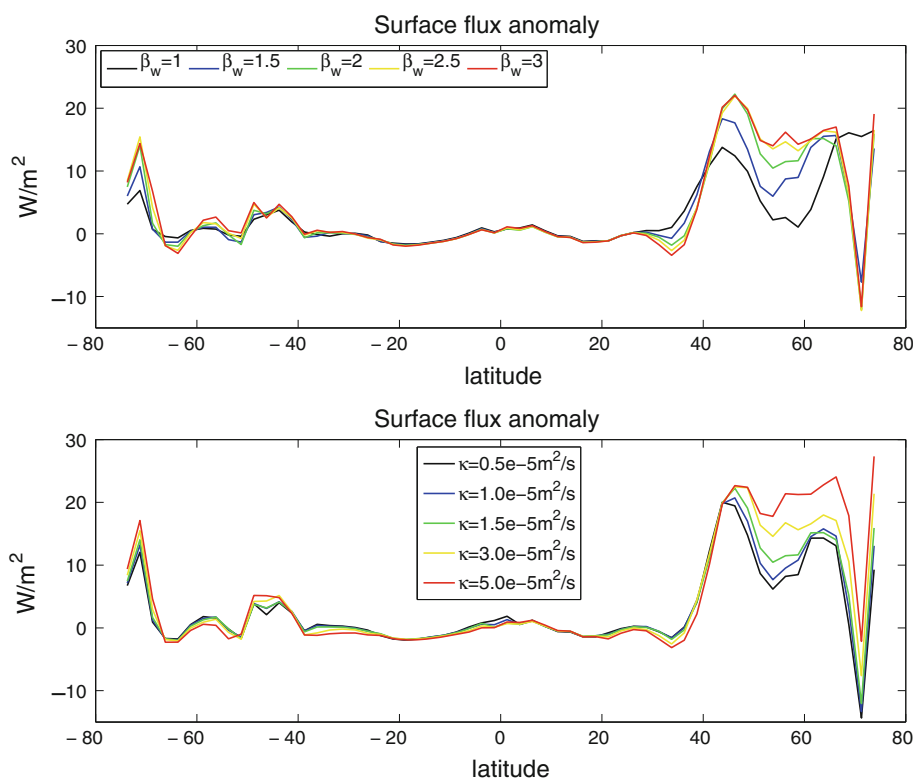


**Fig. 11** 100 years mean, zonal mean surface heat flux anomaly in perturbed runs using the  $\Delta T^*$  and  $\Delta S^*$  forcing calculated from the CM2.1  $2 \times \text{CO}_2$  experiment. Note that  $\beta_s = 1$  for all the integrations here. *Upper* integrations with varied SO wind (set 1 in Table 1). *Lower* integrations with varied vertical diffusivity (set 2 in Table 1)



down the growth of effective system heat capacity via two different ways at the same time, so the overall contribution from  $T'_r$  is hard to estimate.

In the  $T'_a$  field, the ocean also shows different responses under warming and cooling scenarios. Due to lower stratification and a stronger, deeper MOC in cooling experiments relative to the warming experiments, a temperature anomaly signal can go much deeper into the ocean under cooling scenarios (compare lower panels of Figs. 13 and 14). This contributes to the faster growing effective system

heat capacity in the cooling scenarios. In conclusion, our ocean model shows nonlinearity in that in the cooling experiments there is a larger magnitude of MOC change and deeper overturning than in the corresponding warming experiments. This is perhaps not a surprising result given the inherent nonlinearity of convection—a cold, dense surface anomaly will immediately sink giving rise to a circulation anomaly whereas a warm anomaly will float, but it is notable that it does occur in the model. It is possible that seasonal cycle would dilute and ameliorate this

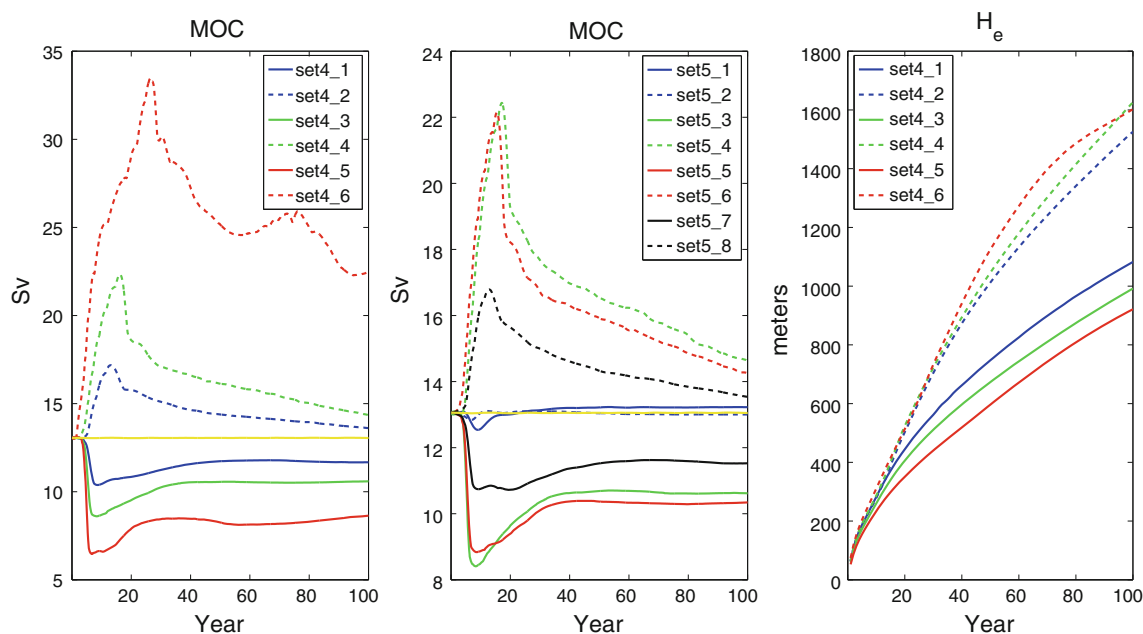


**Fig. 12** Time series for MOC strength (maximum of overturning stream function) and ocean effective depth  $H_e$ . *Left* MOC strength in set 4 experiments (see Fig. 2 and Table 1), yellow line is the CTL run

value. *Middle* MOC strength in set 5 experiments. *Right* effective depth  $H_e$  for set 4 experiments. Cooling experiments have dashed lines

effect somewhat and make the responses more linear, and investigating this is a topic for future study.

### 5 Discussion and interpretation

One robust conclusion of our experiments is that the redistribution of the existing heat reservoir, due to circulation changes acting on the pre-existing temperature field, is as or more important than the quasi-passive contribution of anomalous heat uptake and its advection by the existing velocity field. A very simple scaling argument shows that that this result is not unexpected in so far as the advective term for the redistribution,  $\mathbf{v}' \cdot \nabla T$ , will scale in a similar way as the passive advection  $\bar{\mathbf{v}} \cdot \nabla T'$  if changes in the circulation is buoyancy- and mixing-driven. To see this, consider the scaling for the strength of the meridional overturning circulation (e.g., Vallis 2006, section 15.7)

$$\Psi \sim \kappa^{2/3} \left( \frac{\beta b_\delta L^2}{f^2} \right)^{1/3} \tag{15}$$

where  $b_\delta$  is the buoyancy difference that supplies the pressure difference that drives the circulation. That is,  $\Psi = Ab_\delta^{1/3}$  where  $A$  is a time-invariant parameter. In a steady state the horizontal buoyancy difference maps to the vertical temperature difference but during transient (e.g., decadal scale) climate change, the change in the vertical gradient will normally be larger than the change in

horizontal gradient and it is this that will lead to circulation changes.

The ratio of the magnitude of the change in the existing heat reservoir redistribution ( $M_r$ , say) to the magnitude of the change due to passive advection arising from the anomalous heat flux ( $M_a$ , say) is given by

$$\frac{M_r}{M_a} \sim \frac{\Delta \Psi b_\delta}{\Psi \Delta b_\delta} \tag{16}$$

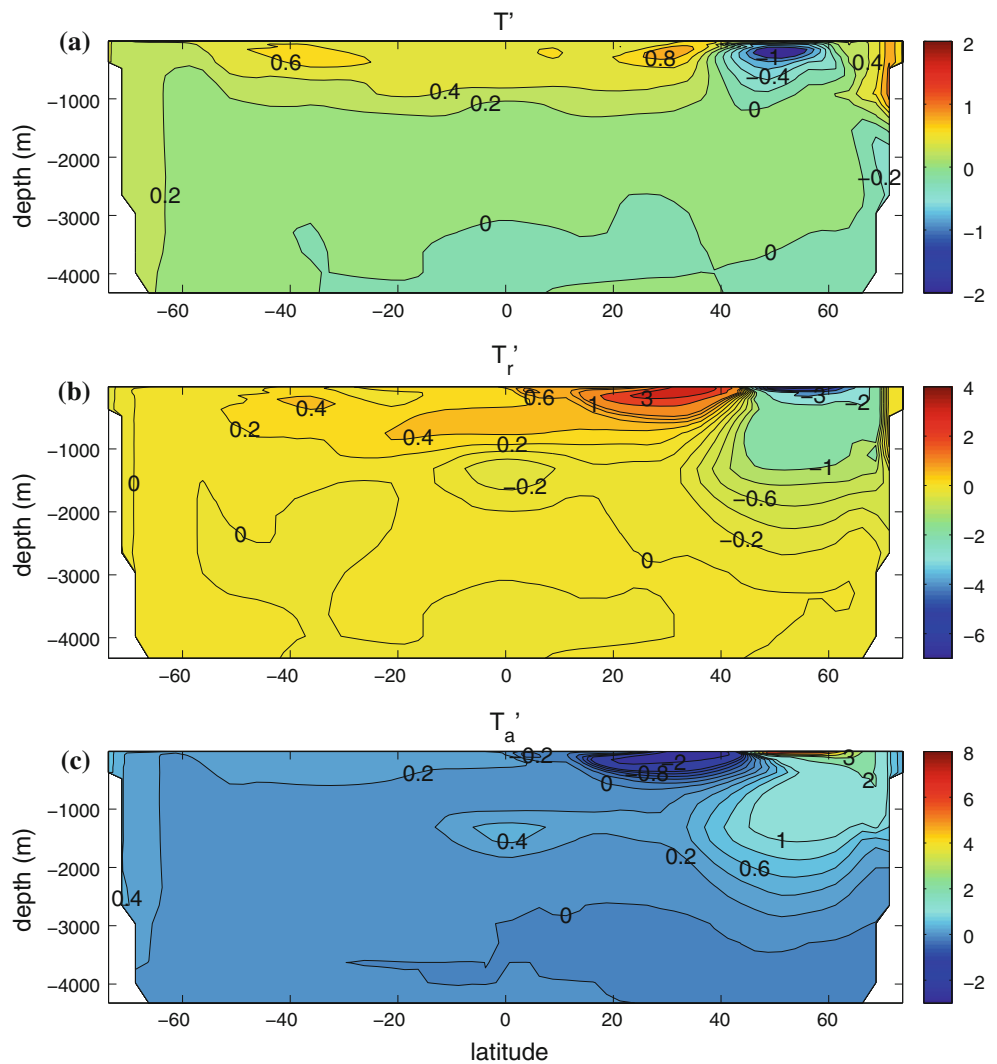
where  $\Delta$  denotes a change caused by the climate change. Using (15) and assuming that the climate changes are small we have  $\Delta \Psi \sim Ab_\delta^{1/3} \Delta b_\delta / 3b_\delta$  and so

$$\frac{M_r}{M_a} \sim \frac{Ab_\delta^{1/3} \Delta b}{3Ab_\delta^{1/3} \Delta b} = O(1). \tag{17}$$

Although the above argument is rather crude and unlikely to provide quantitative guidance, it does suggest that there is no a priori reason why a passive treatment of heat uptake should be quantitatively adequate, at least for the buoyancy-driven circulation. If the circulation is predominantly wind-driven, and not a strong function of the temperature field (as with the wind-driven gyres) then treating the heat uptake in a passive fashion may be a good approximation. Note also that the transient circulation changes may be larger than the changes in the circulation when the deep ocean has finally equilibrated, and at that stage it may be that  $|M_a| \gg |M_r|$ .

We also found that the effective heat capacity of the ocean increases in time. Such an increase is broadly

**Fig. 13** Set 4\_1 experiment (instantaneously warming the ocean surface by  $0.5^{\circ}\text{C}$ , see Fig. 2). **a** zonal mean ocean temperature change  $T'$  in 10th decade. **b** zonal mean existing heat reservoir redistribution  $T'_r$  in 10th decade. **c** Zonal mean contribution from anomalous surface heat flux  $T'_a$ , in 10th decade. The interval of contours is generally  $1^{\circ}\text{C}$  with  $0.2^{\circ}\text{C}$  interval between the  $[-1^{\circ}\text{C}, 1^{\circ}\text{C}]$  range



consistent with the results of Watterson (2000), and indeed might be expected as the deeper ocean partakes in warming, but a quantitative theory is beyond our grasp. In our experiments in which  $\text{CO}_2$  growth rate is roughly linear initially but then levels off, but the growth rate depends on both the Southern Ocean winds and the diffusivity, and given that the circulation itself changes with warming a theory for the heat capacity involves a theory for the circulation itself. Still, the near universal behavior found by Watterson (2000), suggests that a simple approach may be pay dividends.

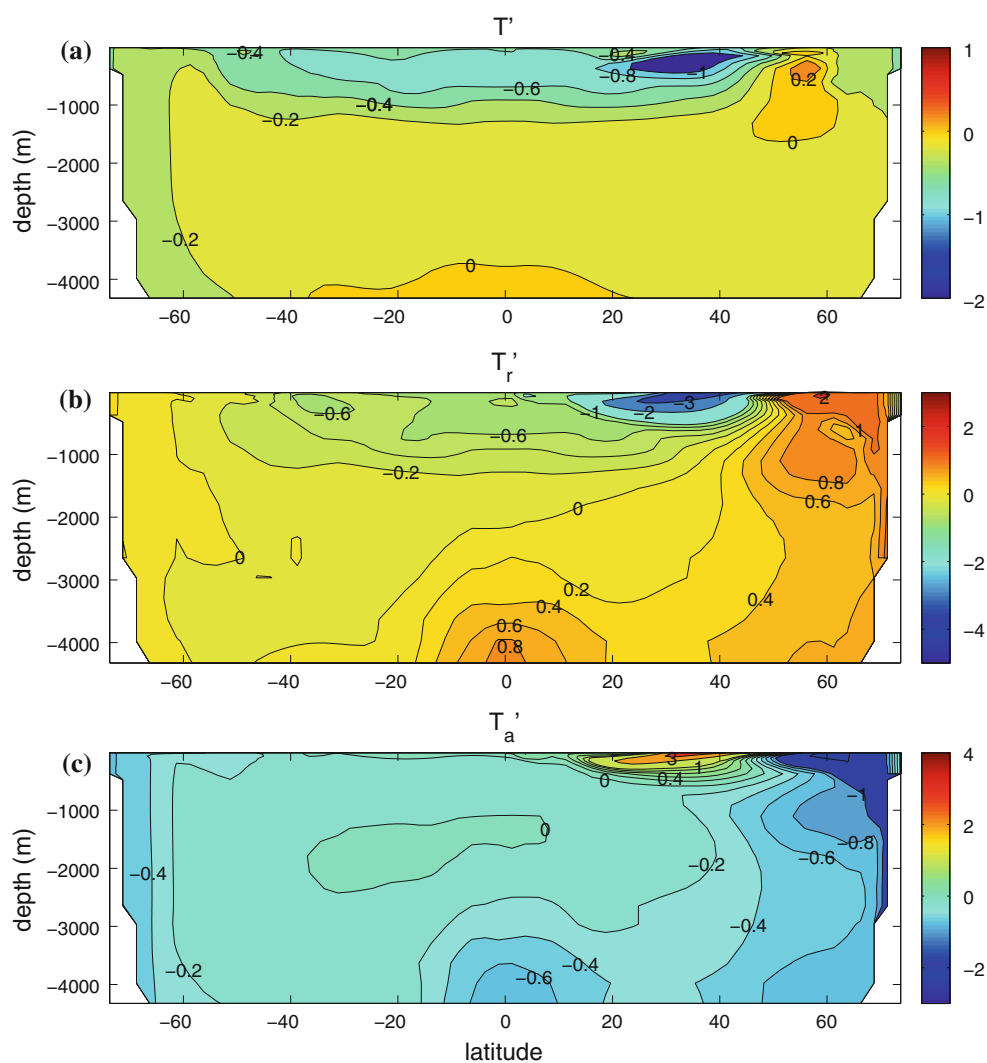
Finally, we found that experiments in which the surface cooled tended to respond more strongly than experiments in which the surface warmed (Fig. 12). This is not surprising in the sense that a cooled surface will tend to convect and communicate the anomaly to depth quite quickly, whereas a warmed surface can only communicate through diffusion. The difference is important, because it suggests that, for example, the response to the radiative forcing of volcanoes is not a good indicator of the response

to global warming. However, the real climate system may be more linear, because of the effects of a seasonal cycle and natural variability. Experiments with a more realistic model are needed to explore this.

## 6 Summary and conclusions

In this paper we have described many experiments carried out with a non-eddy resolving primitive equations ocean model configured in an idealized domain that resembles the Atlantic. We first integrated the model to equilibrium several times, obtaining many different equilibrium states with various values of diapycnal diffusivity, Southern Ocean winds etc. We then performed several different ‘global warming’ experiments on each of these. Some of our warming experiments drew the surface conditions from a warming experiment with a comprehensive coupled climate model whereas others were much more idealized.

**Fig. 14** Set 4\_2 experiment (instantaneously cooling the ocean surface by  $0.5^{\circ}\text{C}$ , see Fig. 2). **a** zonal mean ocean temperature change  $T'$  in 10th decade. **b** zonal mean existing heat reservoir redistribution  $T'_r$  in 10th decade. **c** zonal mean contribution from anomalous surface heat flux  $T'_a$ , in 10th decade. The interval of contours is generally  $1^{\circ}\text{C}$  with  $0.2^{\circ}\text{C}$  interval between the  $[-1^{\circ}\text{C}, 1^{\circ}\text{C}]$  range



We robustly found that the existing heat reservoir redistribution was as or more important than the direct contribution from the anomalous surface heat flux in producing the spatial patterns of ocean temperature anomalies. This conclusion holds over a wide range of physical parameters and climate change scenarios, with exceptions occurring only when the circulation changes were very small. For quantitatively accurate calculations for the spatial patterns of ocean warming it is evidently essential to consider the active heat redistribution. Most specifically, we find that when our ocean model is subject to changes in forcing of a magnitude comparable to that one might expect to see in global warming over the coming decades, changes of the existing heat reservoir redistribution,  $T'_r$ , tend to be somewhat larger than those arising from the anomalous surface heat flux  $T'_a$ . It is inadequate to treat the heat uptake as a passive process with an unchanging circulation.

The wide range of parameters for which this conclusion holds, the similarity in ocean warming patterns between

our simple basin and the Atlantic Ocean in the CM2.1 model, and the general consistency of our results with those obtained using a more comprehensive model by Banks and Gregory (2006), suggest that the results are robust and can be carried over to more complicated models under a variety of warming scenarios, at least as regards the Atlantic Ocean. Our conclusions may be slightly overemphasize the importance of heat redistribution, compared with a passive treatment of heat uptake, because our model resembles the Atlantic, in which the MOC is strongest. The MOC and presumably changes in the MOC induced by global warming are weaker in the Pacific Ocean, and there a passive treatment of heat uptake may give quantitatively more accurate results. We also find the response to heating perturbations is nonlinear, in that cooling perturbations lead to a larger response than warming perturbations.

Typically, we find that larger circulation changes lead to relatively larger existing heat reservoir ( $T'_r$ ) changes. Relatedly, experiments with a higher vertical diffusivity

and stronger Southern Ocean wind generally lead to a faster growing effective system heat capacity because of larger circulation changes and the greater ability of the model to take up heat anomalies at high latitudes. Because diffusivity and Southern Ocean winds tend to differ among comprehensive climate models, the impact of the existing reservoir redistribution on the effective system heat capacity could potentially contribute to the spread of climate response among models on long timescales.

The real ocean is coupled to an atmosphere whereas here our atmosphere is forced by a relaxation, and so the structure of the ocean heat uptake in our model may not reflect that of the real system, or even a coupled model, and this is (one) weakness of our study. Still, the qualitative similarity in the patterns of subsurface warming in a comprehensive GCM in our model with the forcing taken from the GCM suggests that the results are not artifactual. Evidently, the warming occurs first in the mixed layer and then, on the multi-decadal timescale, in the main thermocline and southern ocean (Fig. 3), with a potential localized cooling in high northern latitudes due to a weakening of the MOC, with a significant warming of the abyss only on century-to multi-century timescales. Note that a warming of the thermocline only, with a depth of 1 km, produces to a sea-level rise of about 20 cm per degree, and a warming of the entire water column, with a lower average coefficient of thermal expansion but greater volume, translates to a rise of about 50 cm per degree. Thus, understanding how the heat uptake reaches the deep ocean, and on what timescales, is an important problem that we need to better understand. Use of more realistic coupled models, perhaps in conjunction with more idealized ones, is an important next step.

**Acknowledgments** We would like to thank Mike Winton for many conversations on the subject and for a valuable suggestion with regard to the topography of the ocean. We also thank Stephen Griffies and Richard Slater for help with the numerical model and the passive tracer formulation, and Ian Watterson and Jonathan Gregory for their constructive reviews. This work was supported by DOE award DE-SC0005189 and NSF award OCE-1027603.

## References

- Arbic BK, Owens WB (2001) Climatic warming of Atlantic intermediate waters. *J Clim* 14:4091–4108
- Banks HT, Gregory JM (2006) Mechanisms of ocean heat uptake in a coupled climate model and the implications for tracer based predictions of ocean heat uptake. *Geophys Res Lett* 33:L07,608
- Church JA, Godfrey JS, Jackett DR, McDougall TJ (1991) A model of sea level rise caused by ocean thermal expansion. *J Clim* 4:438–456
- Conkright ME, Antonov JI, Baranova O, Boyer TP, Garcia HE, Gelfeld R, Johnson D, Locarnini RA, Murphy PP, O'Brien TD, Smolyar I, Stephens C (2002) World ocean database 2001, vol. 1, introduction, edited by S. Levitus. NOAA Atlas NESDIS 42, U.S. Government Printing Office, Washington DC [CD-ROM]
- Dalan F, Stone PH, Sokolov AP (2005) Sensitivity of the oceans climate to diapycnal diffusivity in an emic. Part II: global warm scenarios. *J Clim* 18:2482–2496
- Delworth T et al (2006) GFDL's CM2 global coupled climate models. Part I: formulation and simulation characteristics. *J Clim* 9:2190–2196
- Dickinson RE, Schaudt KJ (1998) Analysis of timescales of response of a simple climate model. *J Clim* 11:97–106
- Dixon KW, Delworth TL, Spelman MJ, Stouffer RJ (1999) The influence of transient surface fluxes on North Atlantic overturning in a coupled GCM climate change experiment. *Geophys Res Lett* 26:2749–2752
- Fučkar N, Vallis GK (2007) Interhemispheric influence of surface buoyancy conditions on a circumpolar current. *Geophys Res Lett* 34. doi:10.1029/2008GL030379
- Gent PR, McWilliams JC (1990) Isopycnal mixing in ocean circulation models. *J Phys Oceanogr* 20:150–155
- Gregory JM (2000) Vertical heat transports in the ocean and their effect on time-dependent climate change. *Clim Dyn* 16:501–515
- Gregory JM, Mitchell JFB (1997) The climate response to CO<sub>2</sub> of the Hadley Centre coupled AOGCM with and without flux adjustment. *Geophys Res Lett* 24:1943–1946
- Gregory JM, Dixon KW, Stouffer RJ, Weaver AJ, Driesschaert E, Eby M, Fichefet T, Hasumi H, Hu A, Jungclaus JH, Kamenkovich IV, Levermann A, Montoya M, Murakami S, Nawrath S, Oka A, Sokolov AP, Thorpe RB (2005) A model intercomparison of changes in the Atlantic thermohaline circulation in response to increasing atmospheric CO<sub>2</sub> concentration. *Geophys Res Lett* 32:L12,703
- Griffies SM, Harrison MJ, Pacanowski RC, Rosati A (2004) A technical guide to MOM4. GFDL ocean group technical report 5, NOAA/Geophysical Fluid Dynamics Laboratory
- Haney RL (1971) Surface thermal boundary condition for ocean circulation models. *J Phys Oceanogr* 1:241–248
- Held IM, Winton M, Takahashi K, Delworth T, Zeng F, Vallis GK (2010) Probing the fast and slow components of global warming by returning abruptly to preindustrial forcing. *J Clim* 23:2418–2427. doi:10.1175/2009JCLI3466.1
- Hoffert MI, Callegari AJ, Hsieh CT (1980) The role of deep sea heat storage in the secular response to climatic forcing. *J Geophys Res* 85:6667–6679
- Keen AB, Murphy JM (1997) Influence of natural variability and the cold start problem on the simulated transient response to increasing CO<sub>2</sub>. *Clim Dyn* 13:847–864
- Lowe JA, Gregory JM (2006) Understanding projections of sea level rise in a Hadley Centre coupled climate model. *J Geophys Res* 111. doi:10.1029/2005JC003,421
- Lozier MS, Leadbetter S, Williams RG, Roussenov V, Reed MSC, Moore NJ (2008) The spatial pattern and mechanisms of heat-content change in the North Atlantic. *Science* 319:800–803
- Manabe S, Stouffer RJ (1995) Simulation of abrupt climate change induced by freshwater input to the North Atlantic ocean. *Nature* 378:165–167
- Manabe S, Stouffer RJ (1999) The role of thermohaline circulation in climate. *Tellus B* 51:91–109
- Manabe S, Stouffer RJ (2007) Role of ocean in global warming. *J Meteorol Soc Jpn* 85:385–403
- Padilla L, Vallis GK, Rowley C (2011) Probabilistic estimates of transient climate sensitivity subject to uncertainty in forcing and natural variability. *J Clim* (in press)
- Rahmstorf S (1993) A fast and complete convection scheme for ocean models. *Ocean Model* 101:9–11
- Raper SCB, Gregory JM, Osborn TJ (2001) Use of an upwelling-diffusion energy balance climate model to simulate and diagnose A/OGCM results. *Clim Dyn* 17:601–613

- Raper SCB, Gregory JM, Stouffer RJ (2002) The role of climate sensitivity and ocean heat uptake on AOGCM transient temperature response. *J Clim* 15:124–130
- Ruhlemann C, Mulitza S, Lohmann G, Paul A, Prange M, Wefer G (2004) Intermediate depth warming in the tropical Atlantic related to weakened thermohaline circulation: combining paleoclimate data and modeling results for the last deglaciation. *Paleoceanography* 19:1025
- Samelson R, Vallis GK (1997) Large-scale circulation with small diapycnal diffusivity: the two thermocline limit. *J Mar Res* 55:1–54
- Stouffer RJ (2004) Timescales of climate response. *J Clim* 17:209–217
- Talley LD (1999) Some aspects of ocean heat transport by the shallow, intermediate and deep overturning circulations. In: *Mechanisms of global climate change at millennial time scales*, no. 112 in geophysical monograph, American Geophysical Union, pp 1–22
- Toggweiler JR, Samuels B (1998) On the ocean's large-scale circulation near the limit of no vertical mixing. *J Phys Oceanogr* 28:1832–1852
- Vallis GK (2000) Large-scale circulation and production of stratification: effects of wind, geometry, and diffusion. *J Phys Oceanogr* 30:933–954
- Vallis GK (2006) *Atmospheric and oceanic fluid dynamics: fundamentals and large-scale circulation*. Cambridge University Press, Cambridge, UK
- Vellinga M, Wood RA (2002) Global climatic impacts of a collapse of the Atlantic thermohaline circulation. *Clim Change* 54:251–267
- Watterson IG (2000) Interpretation of simulated global warming using a simple model. *J Clim* 13:202–215
- Wigley TML, Raper SCB (1990) Natural variability of the climate system and detection of the greenhouse effect. *Nature* 344:324–327
- Wigley TML, Schlesinger ME (1985) Analytical solution for the effect of increasing CO<sub>2</sub> on global mean temperature. *Nature* 315:649–652
- Winton M (1997) The damping effect of bottom topography on internal decadal-scale oscillations of the thermohaline circulation. *J Phys Oceanogr* 27:203–208